Available online at www.sciencedirect.com

ScienceDirect

Geochimica et Cosmochimica Acta 294 (2021) 174–191

Geochimica et Cosmochimica Acta

www.elsevier.com/locate/gca

Clumped isotope thermometry in bivalve shells: A tool for reconstructing seasonal upwelling

Diana E. Caldarescu [a,b,*], Henrik Sadatzki [a,b], Carin Andersson [c], Priska Schäfer [d], Helena Fortunato [e], A. Nele Meckler [a]

[a] Department of Earth Science, Bjerknes Centre for Climate Research, University of Bergen, 5007 Bergen, Norway
[b] Alfred Wegener Institute Helmholtz Centre for Polar and Marine Research, 27568-27570 Bremerhaven, Germany
[c] NORCE Norwegian Research Centre, Bjerknes Centre for Climate Research, 5838 Bergen, Norway
[d] Institute of Geosciences, Kiel University, 24098 Kiel, Germany
[e] Department of Biological Sciences, Hokkaido University, 060-0810 Sapporo, Japan

Received 6 July 2020; accepted in revised form 19 November 2020; available online 30 November 2020

Abstract

Carbonate clumped isotope thermometry is a powerful tool for reconstructing paleotemperature and paleosalinity. Despite its broad application in biotic and abiotic materials, its use in paleoclimate studies has been limited due to the large amount of material and high precision required for each temperature estimate. In addition, it is still uncertain to what extent the clumped isotope signal is modified during calcification in various organisms. Using an analytical approach that minimizes sample size, we analysed clumped isotopes (Δ_{47}) in two bivalve shells from the upwelling-dominated Gulf of Panama to reconstruct seasonal temperature and salinity variations. Using the high-resolution profiles in $\delta^{18}O_{shell}$, we grouped Δ_{47} measurements into several intervals to obtain robust average temperature estimates. The reconstructed temperatures agree with available observational data at the 95% confidence level, reflecting seasonal temperature changes of at least ~6 °C. By combining bivalve $\delta^{18}O_{shell}$ and Δ_{47}-based temperatures, we obtain realistic estimates of seasonal $\delta^{18}O_{seawater}$ and salinity changes. Our results suggest that clumped isotopes in bivalve shells can be used for seasonal temperature reconstructions and for disentangling the temperature and $\delta^{18}O_{seawater}$ signals in $\delta^{18}O_{shell}$ variations.

Keywords: Clumped isotopes; Oxygen isotopes; *Megapitaria aurantiaca*; *Argopecten ventricosus*; Stable isotope geochemistry; Gulf of Panama; Upwelling

1. INTRODUCTION

Bivalve mollusks are natural recorders of their habitats, as oceanographic fluctuations are reflected in the geochemistry of their accreted carbonate shells (Schöne and Gillikin, 2013; Surge and Schöne, 2013). Bivalve shell chemistry can reveal, for instance, seasonal cycles and the duration and intensity of upwelling cycles (Killingley and Berger, 1979). However, quantification of hydrographic parameters like temperature and salinity is not straightforward, as most proxies reflect multiple overlying influences. To identify upwelling events and quantify their intensities, Killingley and Berger (1979) proposed to use the correlation between oxygen and carbon isotope ratios in mollusk shells. The vertical advection of ^{18}O-enriched and ^{13}C-depleted thermocline water during strong upwelling events changes the chemistry of subsurface and sur-

* Corresponding author at: Department of Earth Science, Bjerknes Centre for Climate Research, University of Bergen, 5007 Bergen, Norway. Alfred Wegener Institute Helmholtz Centre for Polar and Marine Research, 27570 Bremerhaven, Germany
E-mail address: diana.caldarescu@awi.de (D.E. Caldarescu).

https://doi.org/10.1016/j.gca.2020.11.019
0016-7037/

face waters, resulting in negative correlations between $\delta^{18}O_{shell}$ and $\delta^{13}C_{shell}$ (Killingley and Berger, 1979; Tao et al., 2013). Seasonal cycles in $\delta^{18}O$ and $\delta^{13}C$ isotopic ratios related to upwelling events have been observed and confirmed in the carbonate shells of bivalves (e.g., Bemis and Geary, 1996; Sadler et al., 2012; Graniero et al., 2016) and gastropods (e.g., Geary et al., 1992; Tao et al., 2013; Graniero et al., 2017) collected from gulfs along the Pacific side of the isthmus of Panama, an area with strong seasonal upwelling.

Despite the contribution of isotopic ratios to upwelling reconstructions, Bemis and Geary (1996) have noted that the highest values in $\delta^{18}O_{shell}$ and the lowest values in $\delta^{13}C_{shell}$ do not always occur at the same time. Furthermore, the $\delta^{13}C$ ratios in biogenic carbonates can preserve metabolic carbon signatures (so-called "vital effects") complicating dissolved inorganic carbon (DIC) reconstructions (e.g., McConnaughey et al., 1997). Because both temperature and $\delta^{18}O_{seawater}$ variations influence $\delta^{18}O_{shell}$, it is challenging to derive quantitative paleoenvironmental reconstructions from $\delta^{18}O$ alone. Recently, Sadatzki et al. (2019) suggested that based on a link between distinct Li/Ca peaks in bivalve shells and upwelling-driven phytoplankton blooms, Li/Ca ratios work as a proxy for coastal upwelling. However, like stable isotopes, trace elements can be affected by multiple environmental and physiological factors, which are often not well constrained (e.g., Schöne, 2008).

A promising tool for obtaining absolute temperature estimates independent of seawater chemistry is carbonate clumped isotope thermometry (e.g., Ghosh et al., 2006; Henkes et al., 2018). The clumped isotope signal (Δ_{47}), defined as the excess abundance of doubly-substituted carbonate isotopologues containing both ^{13}C and ^{18}O, relative to a stochastic distribution, is directly related to the formation temperature of the carbonate mineral (Schauble et al., 2006; Eiler, 2007). The temperature dependence of Δ_{47} has been assessed and validated in bivalves (e.g., Came et al., 2007; Eagle et al., 2013; Henkes et al., 2013; Wacker et al., 2014; Daëron et al., 2019), but its use for reconstructions of seasonality has been so far limited (e.g., Van Plantinga and Grossman, 2018; Ghosh et al., 2018).

Here, we evaluate the use of clumped isotope thermometry in two sub-fossil bivalve shells (*Megapitaria aurantiaca* and *Argopecten ventricosus*) from the Gulf of Panama for reconstructions of seasonal changes in this coastal upwelling area. We first reconstruct seasonal changes in temperature and salinity based on Δ_{47} signatures and high-resolution $\delta^{18}O$ profiles. To test the robustness of Δ_{47}-derived temperatures, we compare the reconstructed temperatures and salinities with instrumental and gridded oceanographic data from the Gulf of Panama. Lastly, we attempt to understand the relative influence of temperature and salinity on $\delta^{18}O_{shell}$ during a seasonal upwelling cycle. This allows us to evaluate the effectiveness of clumped isotopes as a quantitative tool for reconstructing upwelling events and its potential application in paleoclimate studies.

2. SEASONAL UPWELLING IN THE GULF OF PANAMA

The formation of the Isthmus of Panama in the Late Pliocene (~3 Ma) has contributed to significant biotic, oceanographic, and climatic changes (Haug and Tiedemann, 1998; O'Dea et al., 2016). Among these is the appearance of strong trade wind-related upwelling in several gulfs of the Tropical Eastern Pacific, such as the Gulf of Panama (O'Dea et al., 2012). The seasonal variability of oceanographic and climatic parameters in the Gulf of Panama is controlled by shifts in the Intertropical Convergence Zone (ITCZ) low-pressure band. The dry upwelling season occurs between January to April, when the ITCZ is located close to the equator, resulting in northeasterly trade winds over the isthmus of Panama. Due to the low elevation of the central isthmus (Fig. 1), the Gulf of Panama on the Pacific side of the isthmus is subject to enhanced northerly wind stress, resulting in Ekman upwelling (e.g., Fig. 2 in D'Croz and O'Dea, 2007). The northerly trade winds over the isthmus are also strengthened by a high-pressure system that develops over the Caribbean and Gulf of Mexico during boreal winter (Xie et al., 2005). Wind-driven upwelling conditions are typically characterised by low sea surface temperature (<20 °C) and high salinity (>33 psu), reflecting the local thermocline water near the surface, as well as reduced precipitation (D'Croz et al., 1991). D'Croz and O'Dea (2009) observed that cold thermocline water residing at about 60-meter depth shoals to the upper 20 meters during the dry upwelling season, enriching the concentration of nutrients in the surface waters and leading to phytoplankton blooms.

The wet season occurs between May to December when the ITCZ is positioned between 7–15°N promoting high precipitation over Panama and river discharge to the Gulf of Panama. During the wet season, sea surface temperature above 27 °C and salinity below 30 psu are recorded, the water column is stratified, and nutrient input and biological activity are low (D'Croz et al., 1991). The large seasonal difference related to coastal upwelling is well reflected by seasonal sea surface temperature changes of about 9 °C in the upper 30 m (e.g., D'Croz and O'Dea, 2009). Furthermore, the Gulf of Panama is also affected by the El Niño Southern Oscillation (ENSO) variability. For instance, sea surface temperature is subject to positive (negative) anomalies, and upwelling intensity can be substantially reduced (enhanced) during El Niño (La Niña) events (Amador et al., 2006). Given the strong seasonal and interannual variability of sea surface temperature and salinity, the Gulf of Panama is a suitable location to evaluate the use of clumped isotope thermometry for seasonal upwelling reconstructions.

3. MATERIALS AND METHODS

3.1. Collection sites and shell material

Two recently dead bivalve specimens were collected from two locations in the Gulf of Panama (7°30´–9°01´N,

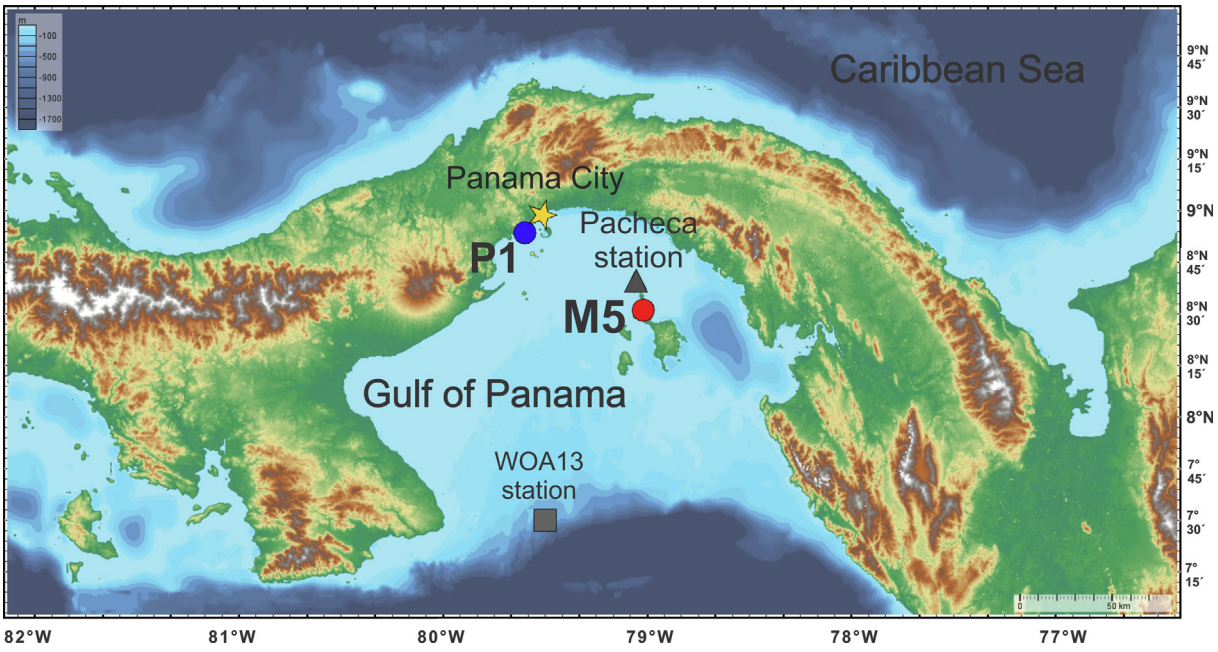

Fig. 1. Bathymetric map of the Gulf of Panama showing the approximate bivalve shell collection sites (red and blue circles). The grey symbols refer to the location of observational data: from the Pacheca station at 6 m depth (triangle; provided by the Smithsonian Tropical Research Institute Physical Monitoring Program) and from station no. 24413 (square; 1° x 1° gridded data from World Ocean Atlas 2013, Locarnini et al., 2013). Panama City (yellow star) is shown as a reference point. (For interpretation of the references to colour in this figure legend, the reader is referred to the web version of this article.)

78°10′–80°40′W) in February 2005. One specimen of *Megapitaria aurantiaca* (Sowerby I, 1831) was collected with intact soft tissues near Casayeta Island, part of Pearl Islands, at a water depth of 5 m (see Sadatzki et al., 2019 for further details) (red circle; Fig. 1). The second specimen, belonging to the species *Argopecten ventricosus* (Sowerby II, 1842), was collected on Venado beach, southwest of Panama City (blue circle; Fig. 1). Both bivalve specimens did not show any encrustations or wear on the shells, indicating they were formed recently.

Megapitaria aurantiaca (M5) is an aragonitic bivalve from the Veneridae family found in bays from California to Ecuador. López-Rocha et al. (2018) mention that it thrives in medium to high energy sandy bottoms and shallow water depths up to 10 meters. *Argopecten ventricosus* (P1) is a calcitic scallop belonging to the Pectinidae family. As our sample was collected on the beach, we lack information regarding water depth and growth temperature. However, this species appears to live in a variety of habitats (e.g., Baqueiro-Cárdenas and Aranda, 2000) and depths up to 90 m (e.g., Medina et al., 2007).

3.2. Sampling and sample treatment

A valve of each specimen (M5 and P1) was embedded in epoxy resin and sectioned along the axis of maximum growth direction in an approximately one cm thick section. The surface of each epoxy section was first ground lightly using a wet silicon carbide paper of grit size P4000 (5 μm) and then polished. The shells were then sonicated with deionized water and air-dried before sampling.

Samples were taken in the outer shell layer using a stationary dental drill (300 μm diameter drill bit) under a stereomicroscope. The sample holes were drilled perpendicular to the daily growth bands in shell M5 (Sadatzki et al., 2019), adjacent to one another (1 cm = 20 drilled holes), starting from the ventral margin (ontogenically oldest) and extending towards the umbo (ontogenically youngest). Depending on the increment width, the samples included carbonate material from at least two growth increments. Although specimen P1 does not present daily growth increments, we applied the same sample spacing strategy as for M5. The sampled section of specimen P1 is 34.5 mm long (1–35.5 mm distance from the ventral margin), and it is 30 mm long in M5 (between 47.5 and 77.5 mm from the ventral margin). Approximately 300 μg of carbonate powder was retrieved from each drilled hole and used for the preparation of two or three aliquots for clumped isotope analyses. In total, 61 samples (168 aliquots) were collected from M5 and 70 samples (135 aliquots) from P1.

The *M. aurantiaca* (M5) specimen used here had been sampled previously along the entire shell for stable isotope and trace element analysis (Sadatzki et al., 2019). For that study, the specimen outer shell layer was micro-drilled every 1 mm from the top of the shell using a hand drilling device, before embedding the specimen in epoxy. For this study, we, in contrast, obtained carbonate samples through micro-drilling holes into the cross-section of the shell.

3.3. Isotope analysis

Individual shell carbonate powder aliquots and carbonate standards of 80–150 µg each were reacted with three drops of 105% phosphoric acid at 70 °C for 360 seconds in an automated Thermo Scientific Kiel IV carbonate preparation device. The resulting CO_2 gas was trapped immediately during the reaction. The gas was then cleaned cryogenically for water and organic contaminants with a custom-made Porapak Q trap. The trap was kept at –20 °C and included silver wool for trapping sulphides following Schmid and Bernasconi (2010). The Porapak trap was cleaned daily by baking at 120 °C for one hour before each analytical session. The purified CO_2 gas was measured on a Thermo Scientific 253Plus mass spectrometer configured to measure CO_2 isotopologues from m/z 44 to 49. Measurements were performed with the long integration dual inlet (LIDI) workflow implemented by Hu et al. (2014), whereby first the sample and then the reference gas was measured over 40 cycles of 10 seconds each under decreasing signal intensity. The reference gas used was limestone CO_2 with an isotopic composition of –5.61‰ (VPDB) for $\delta^{18}O$ and –3.54‰ (VPDB) for $\delta^{13}C$. Each measurement yielded $\delta^{13}C$, $\delta^{18}O$, and δ_{47}, used as the basis to calculate Δ_{47} (e.g., Ghosh et al., 2006).

3.4. Data processing

Four different carbonate standards ETH 1–4 were analysed with the samples and treated in the same manner as the samples. These standards have been previously used and described elsewhere (Meckler et al., 2014; Bernasconi et al., 2018). We applied pressure baseline (PBL) corrections to all signals as suggested by Bernasconi et al. (2013) and Meckler et al. (2014), and used the latest IUPAC recommended parameters for ^{17}O correction (e.g., Brand et al., 2010; Daëron et al., 2016; Schauer et al., 2016). The PBL-corrected results of three of the standards (ETH 1–3) with accepted values by Bernasconi et al. (2018) were used to define the empirical transfer function (ETF), to transfer PBL-corrected Δ_{47} measurements to the absolute reference frame, or carbon dioxide equilibrium scale (CDES) (Dennis et al., 2011). A moving window of 10–30 standards measured both before and after each sample (total N = 20–60, depending on instrument performance) was used for the ETF. The accepted Δ_{47} values of the standards were reported for a 25 °C acid reaction, assuming a difference in acid fractionation between 70 °C to 25 °C of 0.062‰ for Δ_{47} (Defliese and Lohmann, 2015). The acid fractionation factors applied for $\delta^{18}O$ in calcite and aragonite were 1.00871 and 1.00909, respectively (Kim et al., 2007a; Müller et al., 2017). We used aliquots of the fourth carbonate standard (ETH 4) to monitor the stability and performance of our system. During the analytical session of April 27th to August 18th, 2018, the long-term external reproducibility for ETH 4 (Δ_{47} in CDES) was 0.038‰ (1σ, N = 325). The $\delta^{13}C_{shell}$ and $\delta^{18}O_{shell}$ values were drift-corrected with 30 standard measurements of ETH 1, 3, and 4 before and after each measurement (total N = 60) using their isotopic values calibrated against NBS18, NBS19, and LSVEC from Bernasconi et al. (2018). The external reproducibility for the ETH 1, 3 and 4 standards (1σ, N = 970) ranged between 0.047–0.060‰ and 0.022–0.031‰ for $\delta^{18}O$ and $\delta^{13}C$ (VPDB) respectively. The $\delta^{18}O_{shell}$ values were also corrected for scale compression using the same standards. All data processing was done with the "Easotope" software (John and Bowen, 2016), and the results are presented in their standard reference frames, VPDB‰ for $\delta^{18}O_{shell}$ and $\delta^{13}C_{shell}$, and CDES‰ for Δ_{47}. The raw data used for calculating Δ_{47} are available in the EarthChem database (URL: https://doi.org/10.26022/IEDA/111744).

3.4.1. Calculations of Δ_{47}-derived temperature and salinity estimates

The approach we followed for the clumped isotope analysis is optimized for small samples (Meckler et al., 2014; Müller et al., 2017). In contrast to traditional approaches in clumped isotope thermometry that are using larger sample sizes, in the small-sample approach, each replicate measurement is associated with large uncertainty, making it virtually meaningless by itself (Appendix Fig. A1) and requiring averaging over a larger number of measurements. In clumped isotope analysis, the uncertainty is largely due to counting statistics. This uncertainty can be reduced to a meaningful level either by long integration times on the same sample gas or by averaging the values of many individual short measurements on small samples.

In this study, instead of analysing many replicate measurements of the same sample, we averaged the Δ_{47} results retrieved from multiple, adjacent samples, similar to recent work on marine sediments (e.g., Rodríguez-Sanz et al., 2017; Modestou et al., 2020). We applied two different averaging approaches: a LOESS smoothing regression was applied to all data points from each shell (Appendix Fig. A1). In addition, we averaged Δ_{47} measurements for discrete intervals that were significantly different ($p < 0.05$) in the $\delta^{18}O_{shell}$ data. For each of these intervals, outliers in Δ_{47} data were defined as values outside the interquartile range (IQR) multiplied by a factor of 2.2 ($\bar{x}_{replicates} < -3.6423\sigma$ and $\bar{x}_{replicates} > 3.6423\sigma$) (Hoaglin and Iglewicz, 1987), which led to the removal of one outlier for specimen M5 (Appendix Fig. A1). We also did not consider results from samples within abrupt transitions in $\delta^{18}O_{shell}$ for the interval-based Δ_{47} averages (dark grey symbols in Appendix Fig. A1; see also Section 4). The Δ_{47} interval-based averages were translated into temperature estimates using the updated version of the Kele et al. (2015) calibration, recalculated with the IUPAC parameters for ^{17}O correction, as reported in Bernasconi et al. (2018). This calibration equation is based on tufa and travertines and covers a larger temperature range than calibration equations based on biogenic carbonates. It furthermore incorporates data from a few additional biogenic carbonate samples, including the bivalve *Arctica islandica*. The updated Kele calibration was obtained using the same

analytical procedure and similar data processing technique as used in this study, and employed the same carbonate-based standardization scheme. For comparison, we also calculate temperatures with a foraminifera-based calibration equation (Meinicke et al., 2020), which uses the same standardization approach and incorporates a large amount of data from multiple laboratories.

To extract the $\delta^{18}O_{seawater}$ signal from $\delta^{18}O_{shell}$ using Δ_{47} temperatures, we used the synthetic aragonite-water equation by Kim et al. (2007b) for the aragonitic specimen M5 and the synthetic calcite-water equation by Kim and O'Neil (1997) for the calcitic specimen P1 (for equations used, see supplementary material; Fig. S1). For M5, we additionally calculated the $\delta^{18}O_{seawater}$ and salinity values with the biogenic aragonite calibration by Grossman and Ku (1986) modified by Hudson and Anderson (1989) (see supplementary material; Table S1). The $\delta^{18}O_{shell}$ values were converted to VSMOW using the IUPAC conversion (e.g., Brand et al., 2014; Kim et al., 2015). Salinities were calculated from reconstructed $\delta^{18}O_{seawater}$ using an empirically derived equation for surface waters in the Gulf of Panama (Graniero et al., 2017).

Analytical uncertainties on Δ_{47} temperatures, $\delta^{18}O_{shell}$, $\delta^{18}O_{seawater}$, and salinity values are displayed as 95% confidence levels (CI) ($\alpha = 0.05$) following the recommendations by Fernandez et al. (2017). We estimated the temperature, $\delta^{18}O_{seawater}$ and salinity errors at a 95% confidence level using the approach recommended by Schmidt (1999).

4. RESULTS

4.1. Traditional isotopes: $\delta^{18}O$ and $\delta^{13}C$

The analysed samples from the *M. aurantiaca* specimen (M5) range from –4.64 to –1.17‰ in $\delta^{18}O_{shell}$ and from –0.19 to 0.78‰ in $\delta^{13}C_{shell}$. The overall range is thus 3.47‰ for $\delta^{18}O_{shell}$ and 0.97‰ for $\delta^{13}C_{shell}$. In the *A. ventricosus* specimen (P1), the values range from –2.46 to –0.12‰ in $\delta^{18}O_{shell}$ and from –0.59 to 0.82‰ in $\delta^{13}C_{shell}$, giving an overall range of 2.34‰ in $\delta^{18}O_{shell}$ and 1.41‰ in $\delta^{13}C_{shell}$. The $\delta^{18}O_{shell}$ profiles of M5 and P1 show one cycle each (Fig. 2), suggesting that the investigated shell sections reflect approximately one annual cycle.

Both M5 and P1 show clear seasonal $\delta^{18}O$ cycles, each with a dry upwelling season (high $\delta^{18}O_{shell}$) surrounded by significantly lower values ($p < 0.05$; two-tailed Mann-Whitney test) precipitated during wet seasons (Fig. 2A, 2C). The transition between these regimes is, in some cases, abrupt, but plateau-shaped intermediate $\delta^{18}O_{shell}$ values are also observed. The presence of step-wise transitions in the $\delta^{18}O_{shell}$ values aids in dividing the data into several intervals for averaging Δ_{47} (Section 3.4.1 and Table 1). We also calculate interval-based $\delta^{18}O_{shell}$ averages and remove $\delta^{18}O_{shell}$ replicates, which deviate from the sample mean (Fig. 2). While $\delta^{13}C_{shell}$ values are not the focus of this study, we note that intermediate $\delta^{13}C$ values and transition steps are less pronounced in $\delta^{13}C_{shell}$ and seem to occur at a later stage than the ones observed in $\delta^{18}O_{shell}$ (Appendix Fig. A2; supplementary Table S2).

Table 1
Oxygen isotope and clumped isotope (Δ_{47}) composition of shell specimens M5 and P1, averaged per interval (Fig. 2), as well as calculated temperatures and salinities. N is the number of measurements used in each interval.

	Sample no. from shell margin	$\delta^{18}O_{shell}$ (‰)		Δ_{47} (‰)		T (°C)		$\delta^{18}O_{seawater}$ (‰)		S (psu)		N
		Average	*95% CI*	*Average*	*95% CI*	*Average*	*95% CI*	*Average*	*95% CI*	*Average*	*95% CI*	
M5	115–122	–4.14	0.15	0.651	0.012	31.4	3.7	–1.26	0.72	28.8	3.0	23
	123–133	–3.54	0.04	0.658	0.014	29.2	4.2	–1.10	0.82	29.5	3.4	27
	134–144	–2.28	0.11	0.671	0.012	25.4	3.5	–0.58	0.72	31.6	3.0	31
	145–151	–1.42	0.08	0.681	0.018	22.3	5.1	–0.34	1.05	32.6	4.3	21
	153–161	–2.78	0.09	0.665	0.014	27.1	4.1	–0.74	0.82	31.0	3.4	24
	162–170	–3.38	0.05	0.657	0.016	29.5	4.8	–0.87	0.94	30.4	3.9	24
	171–175	–3.92	0.04	0.649	0.018	32.0	5.6	–0.93	1.08	30.2	4.5	14
	Total average	***–2.99***		***0.664***		***27.5***		***–0.87***		***30.4***		***164***
P1	2–18	–1.14	0.15	0.680	0.019	22.6	5.6	0.77	1.16	37.2	4.4	33
	19–49	–0.40	0.04	0.699	0.014	17.4	3.8	0.42	0.82	35.7	3.7	61
	51–71	–2.10	0.08	0.678	0.016	23.3	4.7	–0.06	0.97	33.8	4.1	39
	Total average	***–1.08***		***0.688***		***20.3***		***0.34***		***35.4***		***133***

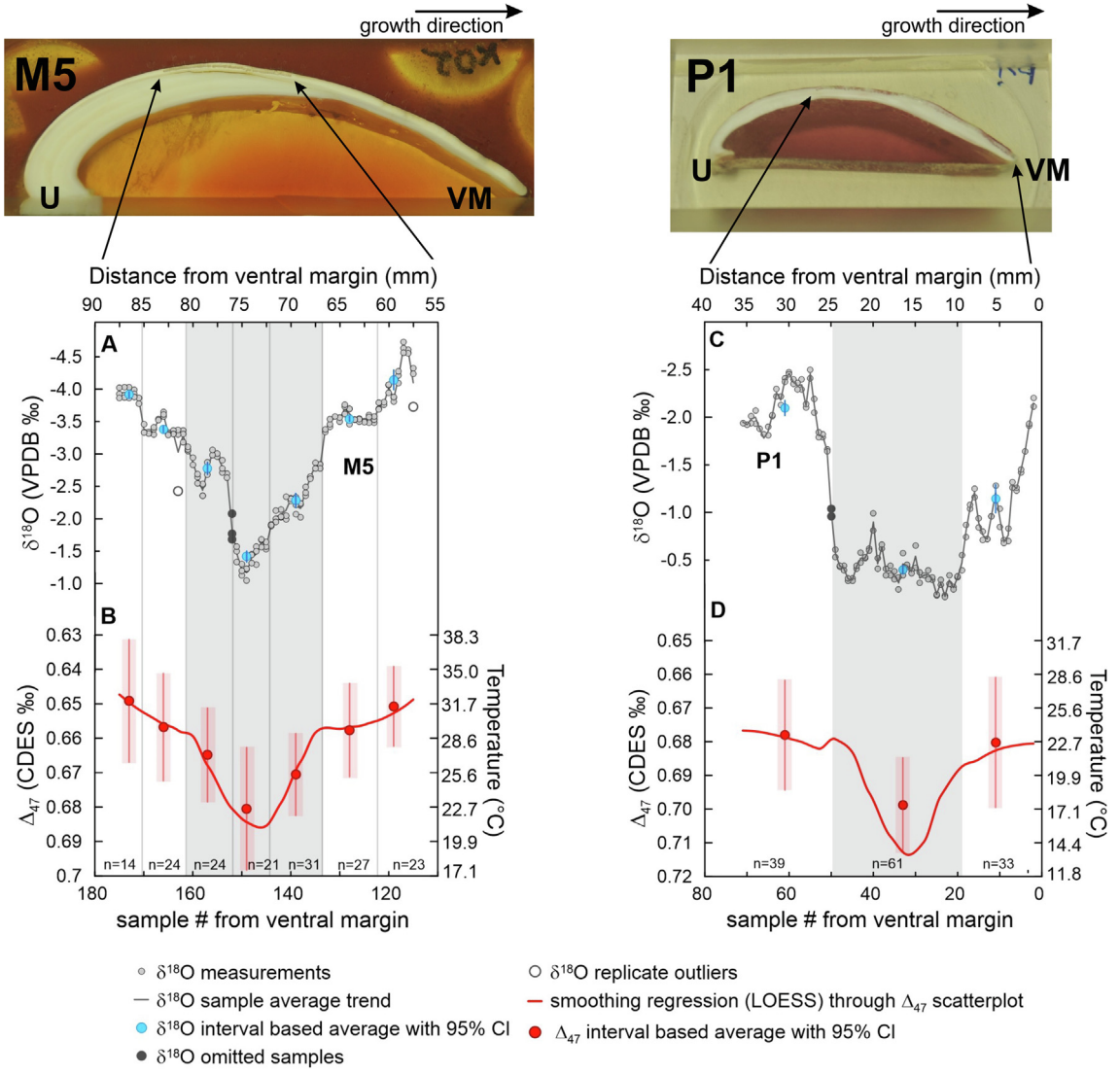

Fig. 2. Oxygen isotope and clumped isotope compositions of the bivalve shells M5 (left) and P1 (right). (A) and (C) show the $\delta^{18}O_{shell}$ record in M5 and P1, respectively. At least two replicates of each carbonate sample were analysed and displayed here as grey data points. Two replicates in two different $\delta^{18}O_{shell}$ samples deviated substantially from the sample mean and were removed (empty circles). The dark grey line connects the mean $\delta^{18}O_{shell}$ per sample. Following the step-wise changes occurring in $\delta^{18}O_{shell}$, we defined several intervals (separated by vertical grey lines) for which measurements are averaged (blue data points with error bars). Samples in abrupt transitions (dark grey points) were omitted for averaging. Note that the $\delta^{18}O_{shell}$ and D_{47} axes are reversed. (B) and (D) illustrate Δ_{47} interval-based averages (red points) and the number of measurements used. Error bars represent 95% confidence level. A LOESS smoothing function (span = 0.5) was applied through all Δ_{47} data (red line; see also Appendix Fig. A1). The grey intervals represent the most ^{18}O-enriched sections in each shell and correspond to the upwelling season. The growth direction (topmost arrows) and the position of the umbo (U) and ventral margin (VM) are indicated on the shell images. (For interpretation of the references to colour in this figure legend, the reader is referred to the web version of this article.)

4.2. Clumped isotope temperatures

The mean Δ_{47}-derived temperature obtained by averaging all analysed samples is 27.5 °C for the aragonitic bivalve M5 and 20.3 °C for the calcitic specimen P1. Seven Δ_{47}-derived average temperatures obtained for M5 and three for P1 (Table 1) are consistent with the temperature curve obtained from the LOESS smoothing (Fig. 2; Appendix Fig. A1). In the sections with the lowest $\delta^{18}O$ values, the aragonitic and calcitic bivalves record the highest temperatures of 32.0 ± 5.6 °C and 23.3 ± 4.7 °C, respectively. The ^{18}O-enriched sections show the lowest temperature estimates: 22.3 ± 5.1 °C for M5 and 17.4 ± 3.8 °C for P1. The gradual seasonal transitions observed in specimen M5 yield intermediate temperature estimates between 25.4 ± 3.5 °C and 27.1 ± 4.1 °C.

When using the foraminifera-based, multi-laboratory calibration by Meinicke et al. (2020), we obtain very similar

temperatures (see supplementary material; Table S3), with differences between −0.2 °C (coldest temperature in P1) and +0.4 °C (warmest temperature in M5).

5. DISCUSSION

5.1. Seasonal ranges in $\delta^{18}O_{shell}$ and calcification temperatures

In seasonal coastal upwelling systems such as the Gulf of Panama, the oxygen isotopic signature derived from molluscan carbonate features prominent seasonal $\delta^{18}O_{shell}$ cycles. Tao et al. (2013) proposed that $\delta^{18}O_{shell}$ ranges can be used as an indicator for upwelling strength with amplitudes exceeding 2‰ reflecting strong upwelling. Here we reconstruct $\delta^{18}O_{shell}$ ranges that exceed the proposed threshold, confirming the mentioned premise. Our results are similar to reported $\delta^{18}O_{shell}$ ranges for *Megapitaria* and *Chione* bivalves (Bemis and Geary, 1996), *Strombus* gastropods (Geary et al., 1992), and *Conus* gastropods (Tao et al., 2013; Graniero et al., 2017) from the Gulf of Panama. However, the negative $\delta^{18}O$—$\delta^{13}C$ correlation suggested to be characteristic for upwelling (e.g., Sadler et al., 2012; Tao et al., 2013; Graniero et al., 2017) is not observed with our dataset (Appendix Fig. A3), indicating that this approach may not always be suitable for reconstructing upwelling events.

The clumped isotope temperature estimates yield seasonal ranges of up to 9.6 ± 3.6 °C in M5 and 5.8 ± 1.7 °C in P1. The seasonal temperature signal recorded by specimen M5 is significant ($p < 0.05$; two-tailed Mann-Whitney test). Although shell P1 records a significant seasonal $\delta^{18}O_{shell}$ signal ($p < 0.05$; see Section 4.1), the temperature signal is barely significant at a 95% confidence level, but statistically significant at lower levels ($p = 0.051$; two-tailed Mann-Whitney test). We attribute the reduced significance of the seasonal temperature difference in P1 to the reduced amplitude of the signal caused by the deeper habitat of this species (see Section 5.2).

5.2. Comparison with observational data

One of our main objectives was to evaluate the use of clumped isotope thermometry for producing reliable estimates of past seasonal temperatures in regions with seasonal upwelling. We suggest possible age models for the two specimens to compare the reconstructed calcification temperatures to observational temperature time series. Since both bivalve specimens were collected dead, we do not have a temporal anchor for sclerochronological analysis. According to Sadatzki et al. (2019), the *Megapitaria aurantica* specimen (M5) records daily growth increments, and the lifespan of this specimen, based on the increment counts and the number of cycles in $\delta^{18}O_{shell}$, was at least four years. In our study, the sampled section of M5 corresponds to approximately one annual cycle. M5 contains 80 distinct growth lines in the ^{18}O-enriched shell section measured here, corresponding to 80 calendar days (e.g., Fig. 3B in Sadatzki et al., 2019). We interpret this section to cover most of the upwelling season, including the peak upwelling in February and March, with the remaining days assigned to late January and the beginning of April (Fig. 3A). Since the wet season is longer and more stable, it is more difficult to assign the remaining calendar days to the ^{18}O-depleted sections. Precise age control is, however, also less important for these shell sections due to the stable temperature during the wet season. We assume the bivalve M5 precipitated calcium carbonate continuously and that the decrease in growth increments width shown in Fig. 3A (presumably between May and October) is likely due to the decline in growth with ontogeny and reduced nutrient availability.

For specimen P1, we also assume continuous growth throughout the year. By analogy with findings from M5, we argue that the shell section with high $\delta^{18}O$ and low Δ_{47}-derived temperature represents the cold upwelling season, from January to April. As the $\delta^{18}O_{shell}$ for P1 presents an almost complete annual cycle, we can also build a temporal framework for this specimen (Fig. 3B).

As we do not have information about the precise calendar years covered by the time series from the two shells, we rely on long oceanographic time series for comparisons and compute monthly averages. Reconstructed clumped isotope temperatures obtained for specimen M5 are compared to temperatures at 6 m depth from a nearby monitoring station (Pacheca station; Fig. 3A). Monthly averages were compiled for the period 2000–2005. This period likely encompasses the lifespan of the aragonitic specimen M5, given its collection date and ontogenetic age. In general, Δ_{47}-derived temperature estimates recorded by M5 agree well with instrumental temperature data. Reconstructed and observed temperatures match best during peak upwelling months (i.e., February and March), while reconstructed temperature estimates during the rainy season are about 2–4 °C warmer than water temperatures recorded at the Pacheca station (Fig. 3A).

The lower clumped isotope temperatures and reduced seasonal amplitude recorded in P1 compared to M5 suggest that this specimen lived at a greater depth relative to M5. However, the exact habitat depth of P1 is unknown. For comparison between reconstructed and observed temperatures, we use monthly average temperature and salinity data extracted from World Ocean Atlas (WOA) 2013 (station no. 24413, slightly offshore at 7°30′N, 79°30′W in Fig. 1) that are available for a range of water depths. Since this station is located in the outer gulf, we evaluated whether temperatures from this station are representative of the inner gulf by comparing the surface temperatures (5 m) to data from Pacheca (6 m) (Appendix Fig. A4.A). The WOA temperatures are up to 3 °C warmer than those at the Pacheca Station during the colder upwelling season, probably because the WOA station is farther away from the coastal upwelling core. However, by using a t-test, we find no significant difference at a 95% statistical level ($p > 0.05$) between the WOA and Pacheca temperatures. Hence, the WOA dataset can be used as a reliable representation of hydrological conditions in the gulf.

The clumped isotope temperatures recorded by specimen P1 during both the upwelling and the rainy seasons show a very good fit to the WOA data from 40 m depth (Fig. 3B). We note that the clumped isotope temperatures

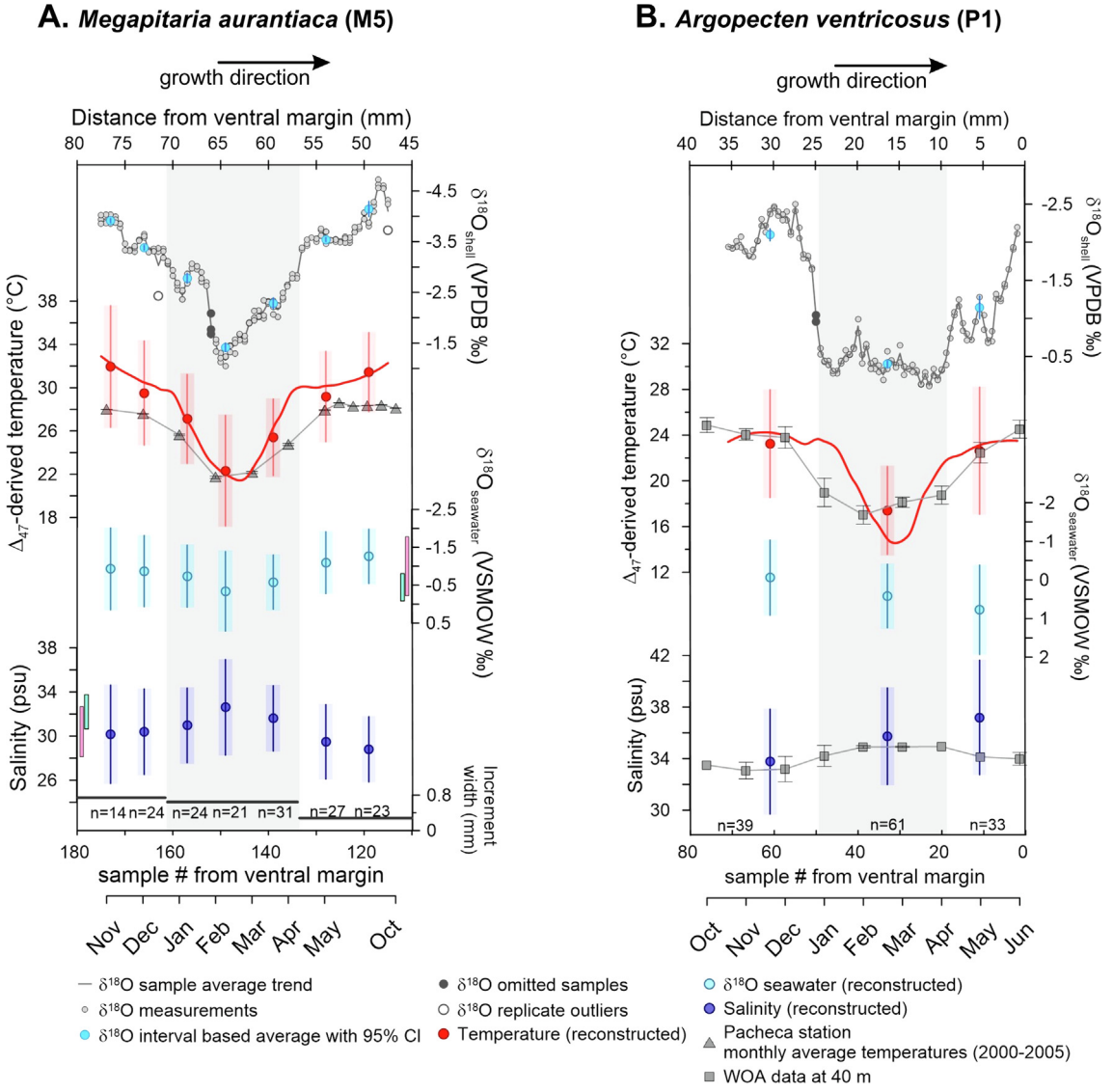

Fig. 3. Temperature and salinity reconstructions using data from M5 (A) and P1 (B). (A) Temperature is compared to monthly average data from the Pacheca station during the period 2000–2005. $\delta^{18}O_{seawater}$ and salinity are compared with seasonal $\delta^{18}O_{seawater}$ and salinity measurements at 7.6 m from the Naos Island Marine Laboratory (green and pink bars indicate the upwelling and non-upwelling seasons, respectively) from Graniero et al. (2017). The age model is based on growth increment counting (see text). The mean growth increment width is shown (for more detail, see Fig. 3B in Sadatzki et al., 2019). (B) Temperature and salinity for P1 are compared to World Ocean Atlas 2013 data at 40 m (Locarnini et al., 2013) (see Appendix Fig. A4.B for data from 30 m depth). The depleted (enriched) section in $\delta^{18}O_{shell}$ (Δ_{47}) corresponds to the dry season. Two to three consecutive months (before and after the upwelling season) are assumed for the wet season to aid comparison with observational data. The grey-shaded intervals represent the upwelling (dry) season lasting from January to April. The error bars (vertical coloured lines) represent the analytical errors (95% CI) of Δ_{47}-derived temperatures and estimated errors of $\delta^{18}O_{seawater}$ and salinity. The arrows along the upper x-axes show the growth direction. Note different scales in panels A and B. (For interpretation of the references to colour in this figure legend, the reader is referred to the web version of this article.)

also agree within the 95% confidence level with temperatures at 30 m depth that are, on average, only 2 °C warmer than those at 40 m (Appendix Fig. A4.B).

5.3. Offsets in Δ_{47}: possible "vital effects?

The clumped isotope temperatures of 22–32 °C recorded by specimen M5 are within the growth temperature range (17–31 °C) of some venerid bivalves (e.g., Goodwin et al., 2001; Schöne et al., 2003). As noted above, however, during the warmest months, the clumped isotope temperature estimates for M5 are consistently slightly higher than the average observational data from the nearby Pacheca station. Instrumental data show minor interannual temperature differences for the warm months, unlike the larger interannual differences of up to 5 °C registered for the upwelling

months, which might be attributed in part to ENSO variability. Hence, the slight temperature offsets in M5 cannot be explained by interannual variability.

It is possible that bivalves exhibit kinetic isotope effects leading to a different clumped isotope disequilibrium than observed in the travertines used for the calibration of Kele et al. (2015), or foraminifera. Some earlier calibration studies on mollusks and brachiopods reported shallower slopes compared to other biogenic and abiogenic carbonates (e.g., Eagle et al. 2013; Henkes et al., 2013), which might be due to the calcification processes in these organisms. However, Came et al. (2014) did not observe such shallow slopes using brachiopods. Similarly, Daëron et al. (2019) report the Δ_{47}-T relationship for three modern bivalve samples, which agrees well with the foraminifera-based calibration from the same laboratory (Peral et al., 2018), obtained with carbonate standardization and included in the combined foraminifera calibration applied here (supplementary Table S3). The observed discrepancies between some of the earlier calibration equations have been suggested to arise from differences in the analytical approach and data processing (Came et al., 2014; Petersen et al., 2019) and the limited temperature range covered by biogenic carbonates, which reduces the robustness of the calibration in the absence of a large number of data points (Fernandez et al., 2017). Therefore, it is still uncertain whether some of these organisms require a different temperature calibration equation for clumped isotopes. Keeping the caveat of the even more limited temperature range of our data in mind, we do not observe a systematic deviation when plotting our data with the data used in the largely abiogenic travertine calibration (Kele et al., 2015; Bernasconi et al., 2018) or the foraminifera based calibration of Meinicke et al. (2020) (Fig. 4), similar to the findings of Came et al. (2014) and Daëron et al. (2019) (light blue data points in Fig. 4). If anything, the slightly overestimated non-upwelling temperatures would suggest a steeper Δ_{47}-T relationship, opposite of what has been suggested by some of the earlier studies on mollusks.

Even if mollusks were generally following the same clumped isotope-temperature relationship, there could be individual cases of biological or "vital" effects. For brachiopods, Bajnai et al. (2018) report a growth-rate dependent kinetic fractionation arising from CO_2 diffusion and incomplete hydroxylation and hydration. In their sample set of modern brachiopods, this "vital" effect led to a positive offset in Δ_{47} (colder temperatures) when compared with a previous Δ_{47} calibration based on brachiopods (Henkes et al., 2013) and a biogenic carbonate Δ_{47} calibration from the same laboratory (Wacker et al., 2014). Similar offsets toward higher Δ_{47} are observed in other types of organisms, such as some coral species (e.g., Saenger et al., 2012; Spooner et al., 2016; Guo et al., 2020) and echinoderms (e.g., Davies and John, 2019). In almost all cases, however, (see Dennis et al., 2013, for an exception), the inferred disequilibrium leads to colder temperatures. In contrast, we observe a minor shift towards warmer-than-expected temperatures during the non-upwelling season, arguing against similar "vital" effects.

Our reconstructed temperatures overlap with measured water temperatures within the experimental error and plot well inside the scatter of the travertine calibration data (Fig. 4). Therefore, the apparent offsets from observational data (Fig. 3) could be due to analytical uncertainty. However, at this stage, we cannot fully rule out a small influence of vital effects on the Δ_{47} temperatures. This remaining uncertainty is because the offsets in M5 seem systematic rather than random. A larger data set covering a larger temperature range will be needed to fully resolve this question. We note that due to the lack of accurate temperature information for P1, we cannot use the data from that specimen to assess potential offsets from calibration data in the same way as with M5. However, as discussed above, the range of temperature estimates is consistent with temperature variability at 30–40 m depth, a likely habitat for *A. ventricosus* species.

5.4. Environmental reconstruction

Using our interval-based Δ_{47} temperatures and $\delta^{18}O_{shell}$ averages, we estimated the seasonal fluctuations in $\delta^{18}O_{seawater}$ and salinity during an upwelling event and parts of the preceding and following rainy seasons. As there are no $\delta^{18}O_{seawater}$ or salinity data from Pacheca station to compare with data from specimen M5, we use surface water observations made at 7.6 m depth from Naos Island (near Panama City) from a recent study by Graniero et al. (2017). The reconstructed seasonal $\delta^{18}O_{seawater}$ signal for M5 of 0.92 ± 0.53‰ corresponds to a seasonal amplitude in salinity change of 3.8 ± 2.2 psu, consistent with the maximal seasonal $\delta^{18}O_{seawater}$ and salinity signals observed at Naos Island of 1.7‰ and 5.7 psu respectively (green and pink bars in Fig. 3A). Absolute reconstructed $\delta^{18}O_{seawater}$ and salinity values for the dry season are on average slightly lower than those measured at Naos Island but well within uncertainty. When using the biogenic calibration equation of Grossman and Ku (1986), we obtain slightly higher $\delta^{18}O_{seawater}$ values (by 0.1–0.2‰) for the wet season, and up to 0.1‰ lower values for the dry season, leading to a smaller seasonal $\delta^{18}O_{seawater}$ and salinity amplitude (see supplementary material; Table S1 and Figs. S2 and S3). The results based on this calibration are still in line with observational data. High-salinity intervals likely reflect both upwelling of more saline subsurface waters to the surface and a reduction of ^{16}O-enriched freshwater input during the dry season (D´Croz and O´Dea, 2007). In turn, increased freshwater input and the lack of upwelling explain the substantially lower surface salinity in the Gulf of Panama during the rainy season. For specimen P1, we compare the reconstructed salinities with WOA data (Fig. 3B). A small seasonal range of 0.48 ± 0.36‰ in $\delta^{18}O_{seawater}$ was reconstructed with this specimen, which equals to 2.0 ± 1.6 psu seasonal change in salinity. The relatively flat seasonal $\delta^{18}O_{seawater}$ signal in P1 compared to the shallow-water bivalve M5 supports a deeper habitat, where salinity changes are minimal. Comparison with monthly salinity data from 40 m depth (i.e., the closest fit to reconstructed temperatures) shows good agreement (Fig. 3B).

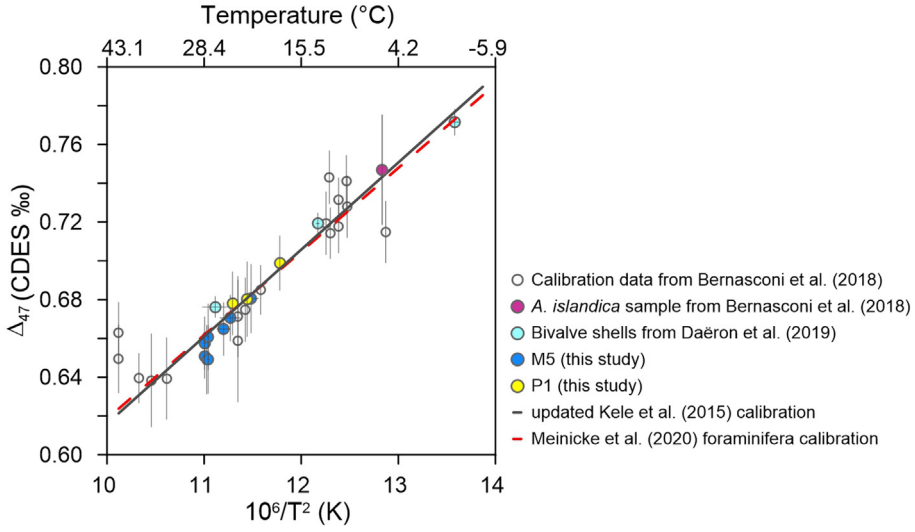

Fig. 4. Temperature dependence of Δ_{47} in tropical bivalve shells compared to calibration data based on travertines and other materials (grey line; Kele et al., 2015; updated by Bernasconi et al., 2018). Growth temperatures for interval-averaged Δ_{47} in specimen M5 (dark blue data points) are assigned using the timeline created in Fig. 3 and averaging the months likely covered by each data-point (i.e., December-November, January, February and March, April, May-August). Although actual growth temperatures are missing for specimen P1, Δ_{47} values and seasonal water temperatures (WOA data) at 40 m (i.e., closest fit to reconstructed temperatures; Appendix Fig. A4) are plotted for comparison (yellow data points). The standard deviations for the compiled months are calculated as the combined variance and used for the 95% confidence interval for temperature. The foraminifera-based calibration (dashed red line; Meinicke et al., 2020) agrees well with the updated Kele calibration (grey line; Bernasconi et al., 2018). Individual calibration data (empty data points) from Bernasconi et al. (2018) are plotted for the temperature interval shown here (6–41.2 °C), and the bivalve sample included in that calibration is highlighted in pink. Bivalve samples from Daëron et al. (2019) are included for comparison (light blue data points). (For interpretation of the references to colour in this figure legend, the reader is referred to the web version of this article.)

The timing and magnitude of temperature versus salinity influence on $\delta^{18}O_{shell}$ through the course of the year can be determined using the independent temperature estimates derived from clumped isotopes (Fig. 5). To isolate the temperature control on $\delta^{18}O_{shell}$, we first transferred the reconstructed temperatures into the corresponding $\delta^{18}O_{shell}$ signal using the average calculated $\delta^{18}O_{seawater}$ for the whole shell in carbonate-water oxygen isotope fractionation equations (see 3.4.1; red data points in Fig. 5). We then computed the residual $\delta^{18}O_{shell}$ response, which reflects variations in $\delta^{18}O_{seawater}$ and a salinity control (blue data points in Fig. 5). Fig. 5A shows that temperature has a dominating influence on $\delta^{18}O_{shell}$ variability in both bivalves, compared with the influence of $\delta^{18}O_{seawater}$ changes on $\delta^{18}O_{shell}$ (red and blue bars in Fig. 5). The strong temperature effect is especially pronounced in the deeper-living specimen P1. For M5, our approach suggests that the large changes in $\delta^{18}O_{shell}$ going into the upwelling season are mostly temperature-driven. However, an increased contribution of the $\delta^{18}O_{seawater}$ signal to $\delta^{18}O_{shell}$ variability is observed during and after the upwelling period for this specimen (Fig. 5A). The temperature decrease and the $\delta^{18}O_{seawater}$ increase confirms the presence of thermocline waters at shallow water depths. The strong temperature effect on $\delta^{18}O_{shell}$ changes during the rainy season contrasts with previous findings by Tao et al. (2013). However, our averaging approach does not allow resolving short-term $\delta^{18}O_{seawater}$ effects on $\delta^{18}O_{shell}$ during rainfall peaks within the rainy season (e.g., Sadatzki et al., 2019).

5.5. Paleoclimate applications

The advantage of using clumped isotope thermometry in biogenic carbonates is that the derived temperature estimates are independent of the $\delta^{18}O$ composition of seawater, which is especially useful in environments experiencing large variations in salinity. Our results show that the application of this method to bivalve shells from the Gulf of Panama allows for the reconstruction of upwelling-driven seasonal temperature variations and provides reasonable salinity estimates. Clumped isotope thermometry does, however, come with a comparatively high level of uncertainty due to limitations by counting statistics. Where possible (i.e., in larger specimens), the error can be further reduced by additional replication. Otherwise, analyses of multiple specimens from the same time interval will increase confidence in reconstructed seasonality.

The application of clumped isotope thermometry on sub-fossil bivalve shells may improve our understanding of upwelling dynamics during different climate and environmental conditions in the past. For instance, the Pliocene epoch is of particular interest in exploring sea surface temperature changes, precipitation patterns related to past ENSO and ITCZ variability, and feedback mechanisms responsible for the deepening of the tropical thermocline (e.g., Fedorov et al., 2006). Seasonal temperatures reconstructed with the clumped isotope method could be valuable to re-evaluate temperature records derived from Mg/

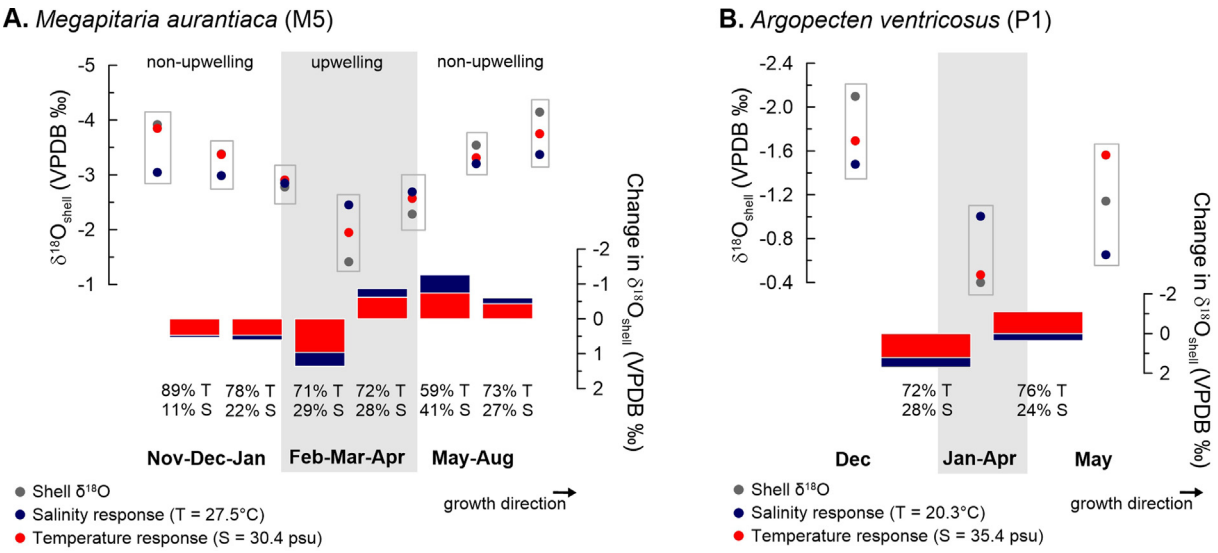

Fig. 5. Temperature and salinity control on shell $\delta^{18}O$ variability over the sampled period (~1 year) for shell M5 (A) and shell P1 (B). The measured average $\delta^{18}O_{shell}$ values are shown as grey data points, whereas the hypothetical $\delta^{18}O_{shell}$ signals corresponding to the average reconstructed temperature and salinity are shown as red and blue data points, respectively. The observed changes in interval-averaged $\delta^{18}O_{shell}$ (in the direction of growth) are split into temperature (red bars) and salinity (blue bars) contributions. (For interpretation of the references to colour in this figure legend, the reader is referred to the web version of this article.)

Ca and alkenones. In the light of our results, the application of clumped isotope thermometry to bivalve shells is promising for paleotemperature and salinity reconstructions on seasonal time scales.

6. CONCLUSIONS

In this study, we used two dead-collected bivalve shells from the Gulf of Panama to test whether clumped isotope thermometry enables the reconstruction of seasonal changes in sea water temperature and oxygen isotope composition in an upwelling regime. The approach used here, namely the distribution of individual Δ_{47} measurements over densely spaced discrete samples following the growth direction, has the distinct advantage of yielding both high-resolution $\delta^{18}O$ (and $\delta^{13}C$) data as well as seasonally resolved Δ_{47} temperatures derived by averaging over neighbouring samples. Temperatures and salinities derived from the aragonitic shell (M5) agree well within 95% uncertainty with observational data from an area nearby the bivalve's habitat (<10 m water depth). A slight warm offset in the non-upwelling season cannot be explained with previously suggested potential "vital" effects, which would bias clumped isotope results towards colder temperatures. The calcitic specimen (P1), whose habitat is unknown but likely deeper, recorded temperatures and salinities that compare well with observational data at water depths of 30–40 m. The $\delta^{18}O_{shell}$ variability observed in the studied specimens stems predominantly from seasonal upwelling-related temperature variations. The effect of $\delta^{18}O_{seawater}$ on $\delta^{18}O_{shell}$ appears to be smaller, with the largest effects close to the surface and during the transition from the upwelling to the non-upwelling season. The application of the clumped isotope method to bivalve shells opens new possibilities for reconstructing past temperature and salinity changes on seasonal timescales, improving our understanding of seasonal coastal upwelling dynamics through time.

Declaration of Competing Interest

The authors declare that they have no known competing financial interests or personal relationships that could have appeared to influence the work reported in this paper.

ACKNOWLEDGEMENTS

We thank Enver Alagoz and Alison Piasecki for technical assistance with clumped isotope measurements, Vilde Melvik, Tamara Trofimova, and Fabian Bonitz for their help during sampling, and Sevasti Modestou and Alvaro F. Bremer for insightful discussions. We are grateful to Ethan Grossman and two other anonymous reviewers, as well as editor Cédric John, whose constructive comments and suggestions helped improving our manuscript. This work was funded by the European Research Council (ERC) under the European Union's Horizon 2020 research and innovation programme (grant agreement no. 638467). H.S. acknowledges financial support through the ERC synergy project 'ice2ice', which received funding from the European Research Council under the European Union´s Seventh Framework Programme (FP7/2007-2013)/ERC grant agreement no. 610055. D.E.C acknowledges financial support from the Center for Climate Dynamics at the Bjerknes Center for Climate Research. We are thankful to the Physical Monitoring Program of the Smithsonian Tropical Research Institute (URL: https://biogeodb.stri.si.edu/physical_monitoring/research/sst) for providing seawater temperature data at the Pacheca station and to government authorities of the Republic of Panama for collection permits.

RESEARCH DATA

The replicate-level raw data of this study are available in the EarthChem library (URL: https://doi.org/10.26022/IEDA/111744).

APPENDIX A

See Figs. A1–A3.

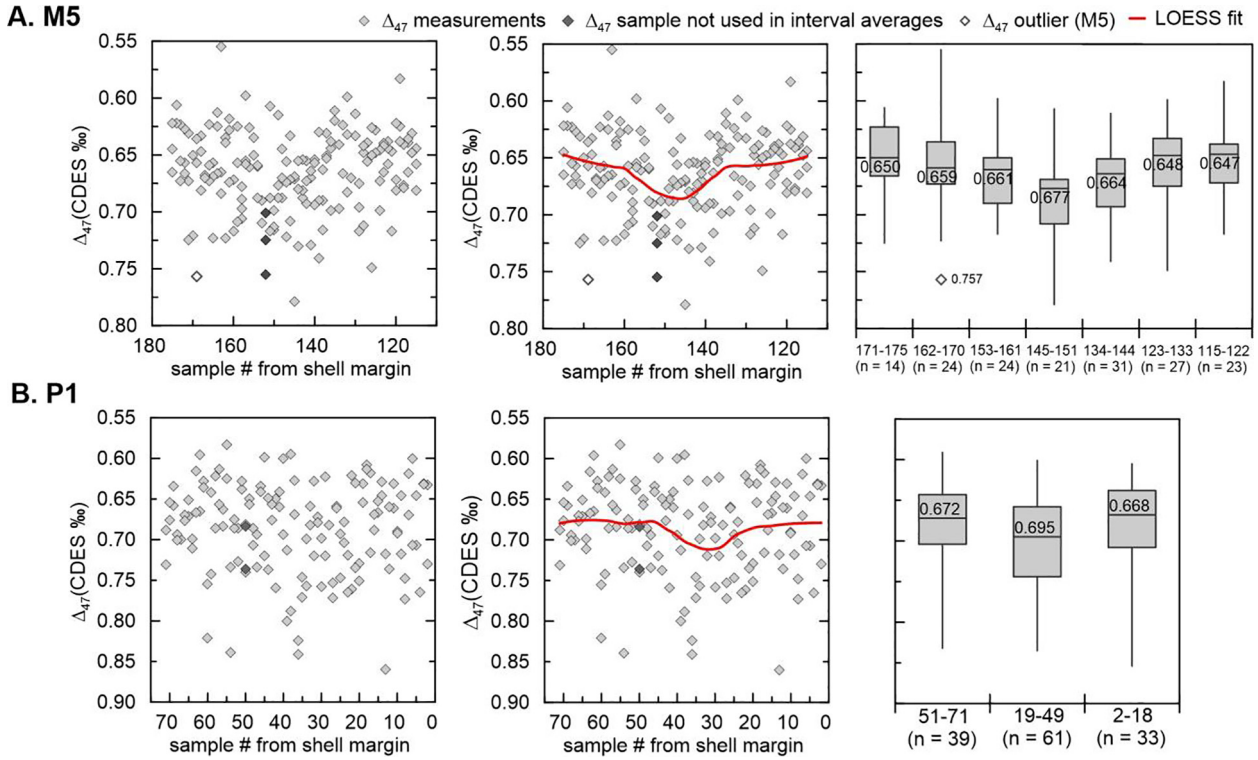

Fig. A1. Replicate-level clumped isotope data from (A) specimen M5 and (B) specimen P1. The scatter corresponds to the expected uncertainty of individual measurements with our small-sample analytical approach (c.f., 1 SD reproducibility of consistency standard of 0.038‰, see methods). The LOESS smoothing applied to mitigate this uncertainty (span = 0.5) is shown in the middle panels. The clumped isotope measurements are alternatively interpreted by averaging results from subsets of data using the $\delta^{18}O$ record to define boundaries (Fig. 2), with boxplots in the right panels showing the distribution of Δ_{47} data and the median values for each group. Note that the Δ_{47} axis is reversed to correspond to the direction of temperature change. The x-axis refers to the sample location in the outer shell layer numbered from the ventral margin (i.e., shell margin) towards the umbo (opposite direction of growth). The dark-grey diamonds represent measurements (from sample #152 for specimen M5; #50 for specimen P1) that were not included in the Δ_{47} interval-based average (c.f., Fig. 2). One outlier (unfilled symbol) was found in the M5 data and excluded by applying a conservative rule (see methods).

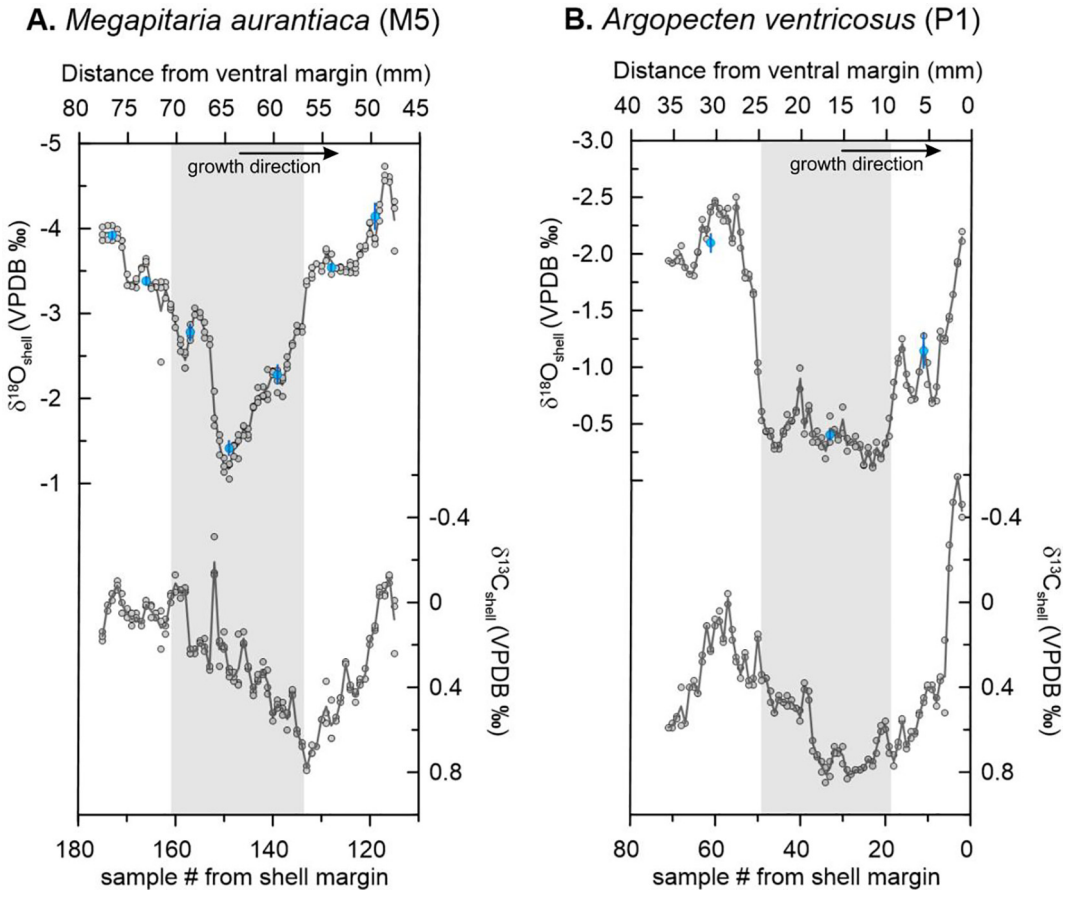

Fig. A2. Comparison of $\delta^{18}O$ and $\delta^{13}C$ shell records from the two bivalve specimens collected from the Gulf of Panama. (A) In shell M5 the $\delta^{18}O$ maximum precedes that in $\delta^{13}C$. However, minima during non-upwelling seasons coincide. (B) In specimen P1, maxima in $\delta^{18}O$ and $\delta^{13}C$ overlap. However, during upwelling, $\delta^{18}O$ is more stable compared to $\delta^{13}C$. Overall, both shells record more gradual $\delta^{13}C$ trends compared to $\delta^{18}O$, lacking abrupt transitions between upwelling and non-upwelling signals. The grey vertical bars represent the upwelling season. Note that the $\delta^{18}O$ and $\delta^{13}C$ axes are reversed. The arrows along the upper x-axes indicate the growth direction.

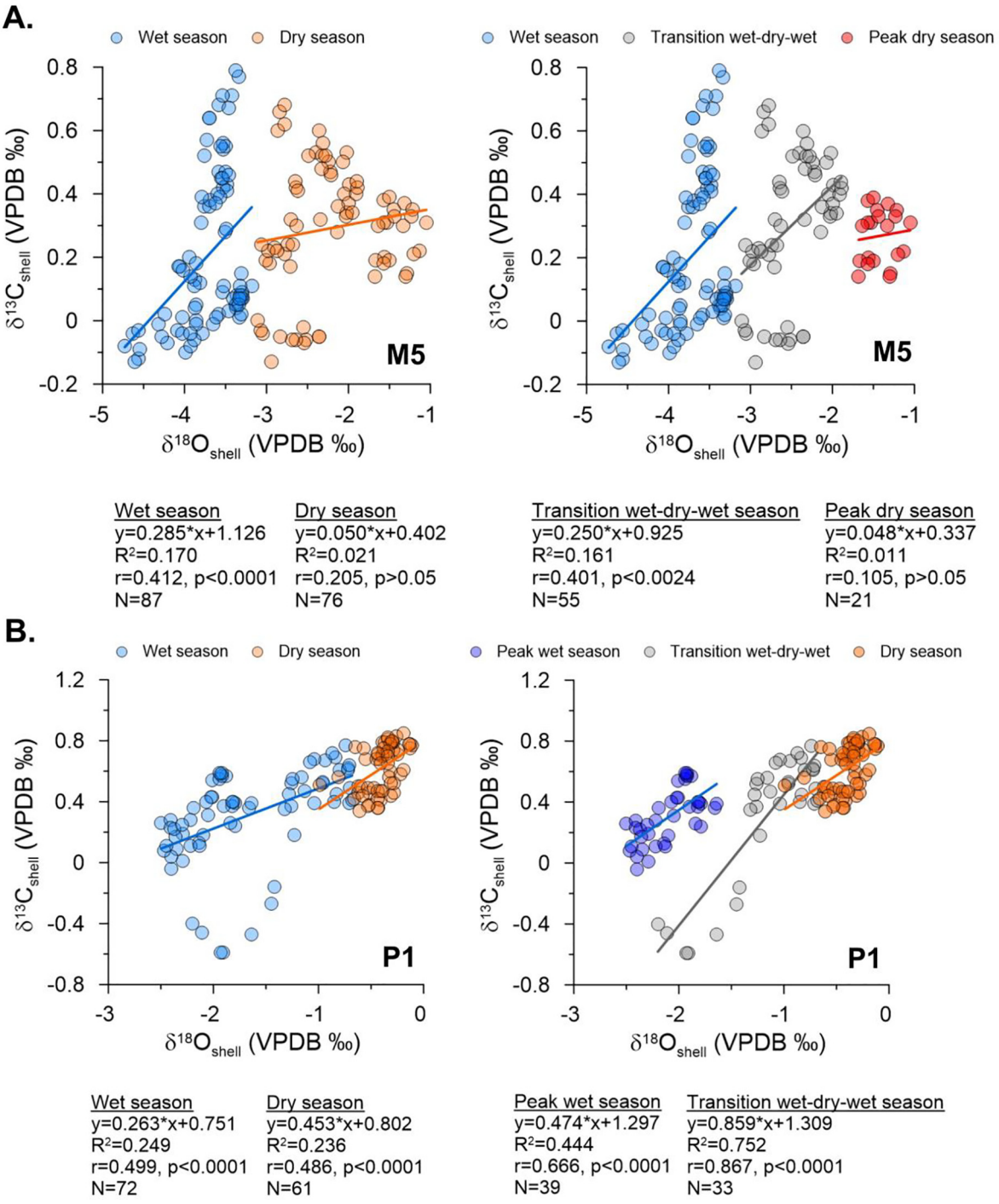

Fig. A3. (A) Shell $\delta^{18}O$–$\delta^{13}C$ plots for *Megapitaria aurantiaca* (M5). The first panel shows the relationship between $\delta^{18}O$–$\delta^{13}C$ during the wet season (blue data points; samples 115–133 and 162–175) and dry season (orange data points; samples 134–161). In the second panel, the wet season contains the same values as in the first panel, whereas the values from the dry season were split into two sections: the ones from peak dry season (red data points; samples 145–151) and from in-between the seasons (grey data points; samples 134–144 and 153–161). Notice that a negative $\delta^{18}O$–$\delta^{13}C$ correlation for the upwelling season is not observed, whereas positive correlations are obtained for the wet season, and for the $\delta^{18}O$ and $\delta^{13}C$ values found in transition between seasons. (B) Shell $\delta^{18}O$–$\delta^{13}C$ plots for *Argopecten ventricosus* (P1). In the first panel, $\delta^{18}O$ and $\delta^{13}C$ values correspond to the wet season (blue data points; samples 2–18 and 51–71) and dry season (orange data points; samples 19–49). In the second panel, the wet season was split into two sections containing $\delta^{18}O$ and $\delta^{13}C$ values from the peak wet season (dark blue points; samples 51–71), and transitioning between dry and wet season (grey data points; samples 2–18). In shell P1, significant and positive $\delta^{18}O$–$\delta^{13}C$ correlations ($r > 0.4$) were found for both the dry and wet season. (For interpretation of the references to colour in this figure legend, the reader is referred to the web version of this article.)

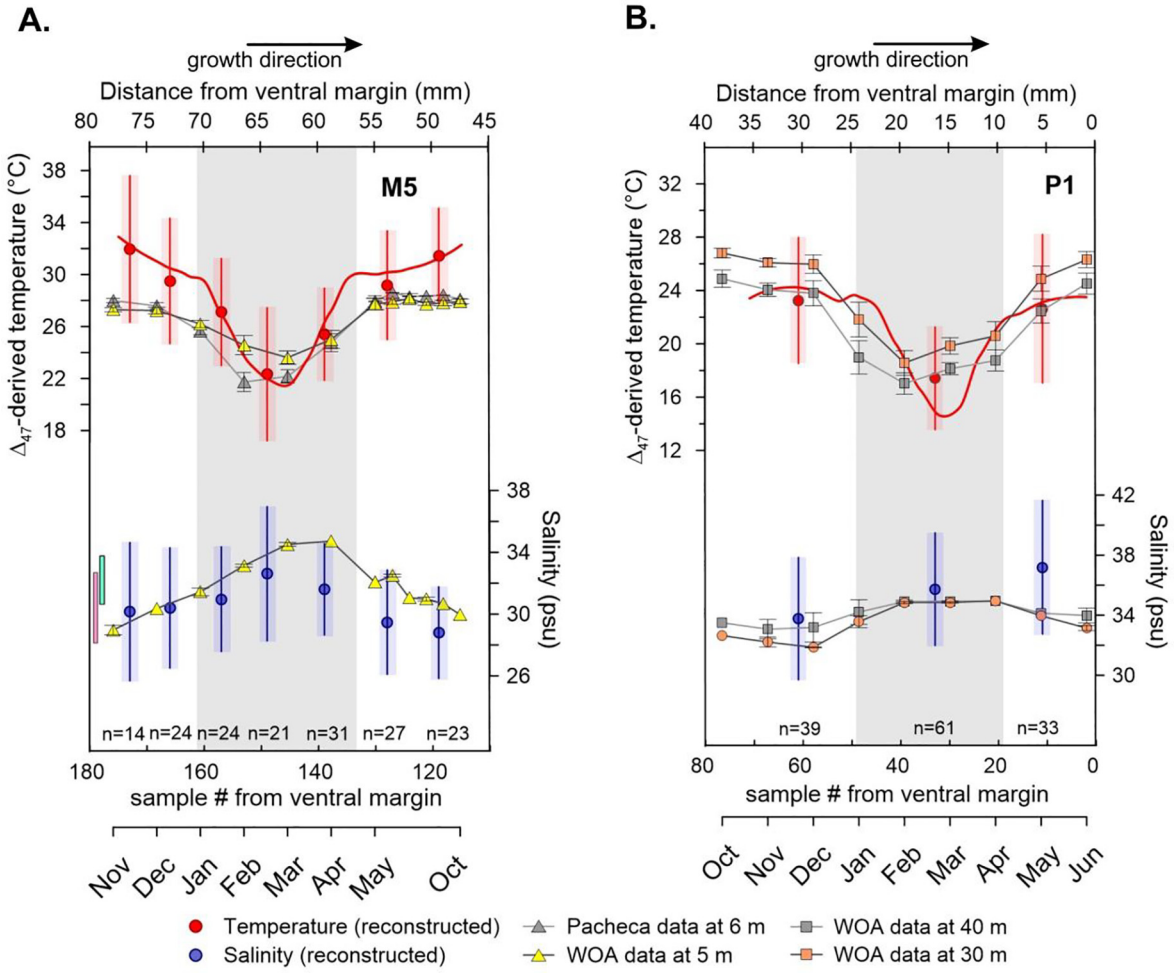

Fig. A4. (A) Comparisons between observed temperature and salinity at Pacheca station (6 m), WOA data (5 m) at station no. 24413, and Δ_{47} data from specimen M5. Salinity measurements from Graniero et al. (2017) are plotted as green (upwelling) and pink (non-upwelling) bars and compared to salinity at station no. 24413 (5 m) and reconstructed salinity in M5. (B) Comparisons between observations of temperature and salinity at 30 and 40 m at station no. 24413 (WOA) and reconstructions from specimen P1. The grey-shaded vertical sections represent the upwelling season, and the red and blue shaded vertical bars show the error bars (95% CI) of reconstructed temperature and salinity. The arrows along the upper x-axes indicate growth direction. (For interpretation of the references to colour in this figure legend, the reader is referred to the web version of this article.)

APPENDIX B. SUPPLEMENTARY MATERIAL

Supplementary data to this article can be found online at https://doi.org/10.1016/j.gca.2020.11.019.

REFERENCES

Amador J. A., Alfaro E. J., Lizano O. G. and Magaña V. O. (2006) Atmospheric forcing of the eastern tropical Pacific: A review. *Prog. Oceanogr.* **69**, 101–142.

Bajnai D., Fiebig J., Tomašových A., Milner G. S., Rollion-Bard C., Raddatz J., Löffler N., Primo-Ramos C. and Brand U. (2018) Assessing kinetic fractionation in brachiopod calcite using clumped isotopes. *Sci. Rep.* **8**, 533.

Baqueiro-Cárdenas E. and Aranda D. A. (2000) A review of reproductive patterns of bivalve mollusks from Mexico. *Bull. Mar. Sci.* **66**, 13–27.

Bemis B. E. and Geary D. H. (1996) The usefulness of bivalve stable isotope profiles as environmental indicators: Data from the eastern Pacific Ocean and the southern Caribbean sea. *Palaios* **11**, 328.

Bernasconi S. M., Hu B., Wacker U., Fiebig J., Breitenbach S. F. M. and Rutz T. (2013) Background effects on Faraday collectors in gas-source mass spectrometry and implications for clumped isotope measurements. *Rapid Commun. Mass Spectrom.* **27**, 603–612.

Bernasconi S. M., Müller I. A., Bergmann K. D., Breitenbach S. F. M., Fernandez A., Hodell D. A., Jaggi M., Meckler A. N., Millan I. and Ziegler M. (2018) Reducing uncertainties in carbonate clumped isotope analysis through consistent carbonate-based standardization. *Geochem. Geophys. Geosyst.* **19**, 2895–2914.

Brand W. A., Assonov S. S. and Coplen T. B. (2010) Correction for the ^{17}O interference in $\delta(^{13}C)$ measurements when analyzing CO_2 with stable isotope mass spectrometry (IUPAC Technical Report). *Pure Appl. Chem.* **82**, 1719–1733.

Brand W. A., Coplen T. B., Vogl J., Rosner M. and Prohaska T. (2014) Assessment of international reference materials for

isotope-ratio analysis (IUPAC Technical Report). *Pure Appl. Chem.* **86**, 425–467.

Came R. E., Brand U. and Affek H. P. (2014) Clumped isotope signatures in modern brachiopod carbonate. *Chem. Geol.* **377**, 20–30.

Came R. E., Eiler J. M., Veizer J., Azmy K., Brand U. and Weidman C. R. (2007) Coupling of surface temperatures and atmospheric CO_2 concentrations during the Palaeozoic era. *Nature* **449**, 198–201.

D'Croz L. and O'Dea A. (2009) Nutrient and chlorophyll dynamics in Pacific Central America (Panama). *Proceedings of the Smithsonian Marine Sciences Symposium.* **38**, 335–344.

D'Croz L. and O'Dea A. (2007) Variability in upwelling along the Pacific shelf of Panama and implications for the distribution of nutrients and chlorophyll. *Estuar. Coast. Shelf Sci.* **73**, 325–340.

D'Croz L., Del Rosario J. B. and Gómez J. A. (1991) Upwelling and phytoplankton in the Bay of Panamá. *Revista de Biología Tropical* **39**, 233–241.

Daëron M., Blamart D., Peral M. and Affek H. P. (2016) Absolute isotopic abundance ratios and the accuracy of Δ_{47} measurements. *Chem. Geol.* **442**, 83–96.

Daëron M., Drysdale R. N., Peral M., Huyghe D., Blamart D., Coplen T. B., Lartaud F. and Zanchetta G. (2019) Most Earth-surface calcites precipitate out of isotopic equilibrium. *Nat. Commun.* **10**, 1–7.

Davies A. J. and John C. M. (2019) The clumped ($^{13}C^{18}O$) isotope composition of echinoid calcite: Further evidence for "vital effects" in the clumped isotope proxy. *Geochim. Cosmochim. Acta* **245**, 172–189.

Defliese W. F. and Lohmann K. C. (2015) Non-linear mixing effects on mass-47 CO_2 clumped isotope thermometry: Patterns and implications. *Rapid Commun. Mass Spectrom.* **29**, 901–909.

Dennis K. J., Affek H. P., Passey B. H., Schrag D. P. and Eiler J. M. (2011) Defining an absolute reference frame for 'clumped' isotope studies of CO_2. *Geochim. Cosmochim. Acta* **75**, 7117–7131.

Dennis K. J., Cochran J. K., Landman N. H. and Schrag D. P. (2013) The climate of the Late Cretaceous: New insights from the application of the carbonate clumped isotope thermometer to Western Interior Seaway macrofossil. *Earth Planet. Sci. Lett.* **362**, 51–65.

Eagle R. A., Eiler J. M., Tripati A. K., Ries J. B., Freitas P. S., Hiebenthal C., Wanamaker A. D., Taviani M., Elliot M., Marenssi S., Nakamura K., Ramirez P. and Roy K. (2013) The influence of temperature and seawater carbonate saturation state on ^{13}C–^{18}O bond ordering in bivalve mollusks. *Biogeosciences* **10**, 4591–4606.

Eiler J. M. (2007) "Clumped-isotope" geochemistry—The study of naturally-occurring, multiply-substituted isotopologues. *Earth Planet. Sci. Lett.* **262**, 309–327.

Fedorov A. V., Dekens P. S., McCarthy M., Ravelo A. C., DeMenocal P. B., Barreiro M., Pacanowski R. C. and Philander S. G. (2006) The pliocene paradox (mechanisms for a permanent El Niño). *Science* **312**, 1485–1489.

Fernandez A., Müller I. A., Rodríguez-Sanz L., van Dijk J., Looser N. and Bernasconi S. M. (2017) A reassessment of the precision of carbonate clumped isotope measurements: implications for calibrations and paleoclimate reconstructions. *Geochem. Geophys. Geosyst.* **18**, 4375–4386.

Geary D. H., Brieske T. A. and Bemis B. E. (1992) The influence and interaction of temperature, salinity, and upwelling on the stable isotopic profiles of Strombid gastropod shells. *Palaios* **7**, 77.

Ghosh P., Adkins J., Affek H., Balta B., Guo W., Schauble E. A., Schrag D. and Eiler J. M. (2006) ^{13}C–^{18}O bonds in carbonate minerals: A new kind of paleothermometer. *Geochim. Cosmochim. Acta* **70**, 1439–1456.

Ghosh P., Prasanna K., Banerjee Y., Williams I. S., Gagan M. K., Chaudhuri A. and Suwas S. (2018) Rainfall seasonality on the Indian subcontinent during the Cretaceous greenhouse. *Sci. Rep.* **8**, 8482.

Goodwin D. H., Flessa K. W., Schone B. R. and Dettman D. L. (2001) Cross-calibration of daily growth increments, stable isotope variation, and temperature in the Gulf of California bivalve mollusk Chione cortezi: Implications for paleoenvironmental analysis. *Palaios* **16**, 387.

Graniero L. E., Grossman E. L. and O'Dea A. (2016) Stable isotopes in bivalves as indicators of nutrient source in coastal waters in the Bocas del Toro Archipelago, Panama. *PeerJ* **4** e2278.

Graniero L. E., Grossman E. L., Robbins J., Morales J., Thompson R. and O'Dea A. (2017) Conus shell $\delta^{13}C$ values as proxies for $\delta^{13}C_{DIC}$ in tropical waters. *Palaeogeogr. Palaeoclimatol. Palaeoecol.* **472**, 119–127.

Grossman E. L. and Ku T. L. (1986) Oxygen and carbon isotope fractionation in biogenic aragonite: Temperature effects. *Chem. Geol.: Isotope Geosci. Section* **59**, 59–74.

Guo Y., Deng W., Wei G., Chen X., Liu X., Wang X., Lo L., Cai G. and Zeng T. (2020) Exploring the temperature dependence of clumped isotopes in modern Porites corals. *J. Geophys. Res.: Biogeosci.* **125**.

Haug G. H. and Tiedemann R. (1998) Effect of the formation of the Isthmus of Panama on Atlantic Ocean thermohaline circulation. *Nature* **393**, 673–676.

Henkes G. A., Passey B. H., Grossman E. L., Shenton B. J., Yancey T. E. and Pérez-Huerta A. (2018) Temperature evolution and the oxygen isotope composition of Phanerozoic oceans from carbonate clumped isotope thermometry. *Earth Planet. Sci. Lett.* **490**, 40–50.

Henkes G. A., Passey B. H., Wanamaker A. D., Grossman E. L., Ambrose W. G. and Carroll M. L. (2013) Carbonate clumped isotope compositions of modern marine mollusk and brachiopod shells. *Geochim. Cosmochim. Acta* **106**, 307–325.

Hoaglin D. C. and Iglewicz B. (1987) Fine-tuning some resistant rules for outlier labeling. *J. Am. Stat. Assoc.* **82**, 1147–1149.

Hu B., Radke J., Schlüter H.-J., Heine F. T., Zhou L. and Bernasconi S. M. (2014) A modified procedure for gas-source isotope ratio mass spectrometry: The long-integration dual-inlet (LIDI) methodology and implications for clumped isotope measurements. *Rapid Commun. Mass Spectrom.* **28**, 1413–1425.

Hudson J. D. and Anderson T. F. (1989) Ocean temperatures and isotopic compositions through time. *Earth and Environmental Science Transactions of the Royal Society of Edinburgh* **80**, 183–192.

John C. M. and Bowen D. (2016) Community software for challenging isotope analysis: First applications of 'Easotope' to clumped isotopes. *Rapid Commun. Mass Spectrom.* **30**, 2285–2300.

Kele S., Breitenbach S. F. M., Capezzuoli E., Meckler A. N., Ziegler M., Millan I. M., Kluge T., Deák J., Hanselmann K., John C. M., Yan H., Liu Z. and Bernasconi S. M. (2015) Temperature dependence of oxygen and clumped isotope fractionation in carbonates: A study of travertines and tufas in the 6–95 °C temperature range. *Geochim. Cosmochim. Acta* **168**, 172–192.

Killingley J. S. and Berger W. H. (1979) Stable isotopes in a mollusk shell: Detection of upwelling events. *Science* **205**, 186–188.

Kim S.-T., Coplen T. B. and Horita J. (2015) Normalization of stable isotope data for carbonate minerals: Implementation of IUPAC guidelines. *Geochim. Cosmochim. Acta* **158**, 276–289.

Kim S.-T., Mucci A. and Taylor B. E. (2007a) Phosphoric acid fractionation factors for calcite and aragonite between 25 and 75 °C: Revisited. *Chem. Geol.* **246**, 135–146.

Kim S.-T. and O'Neil J. R. (1997) Equilibrium and nonequilibrium oxygen isotope effects in synthetic carbonates. *Geochim. Cosmochim. Acta* **61**, 3461–3475.

Kim S.-T., O'Neil J. R., Hillaire-Marcel C. and Mucci A. (2007b) Oxygen isotope fractionation between synthetic aragonite and water: Influence of temperature and Mg^{2+} concentration. *Geochim. Cosmochim. Acta* **71**, 4704–4715.

Locarnini R. A., Mishonov A. V., Antonov J. I., Boyer T. P., Garcia H. E., Baranova O. K., Zweng M. M., Paver C. R., Reagan J. R., Johnson D. R., Hamilton M. and Seidov D. (2013) World Ocean Atlas 2013. Volume 1: Temperature. In NOAA Atlas NESDIS 73 S. Levitus, Ed., A. Mishonov Technical Ed. p. 40.

López-Rocha J. A., Melo F.-J.-F.-R., Gastélum-Nava E., Larios-Castro E. and Romo-Piñera A. (2018) Morphometric relationship, growth parameters, and natural mortality as estimated primary inputs for fishery management in new fishing areas for bivalve molluscs (Bivalvia: Veneridae). *J. Shellfish Res.* **37**, 591–600.

McConnaughey T. A., Burdett J., Whelan J. F. and Paull C. K. (1997) Carbon isotopes in biological carbonates: Respiration and photosynthesis. *Geochim. Cosmochim. Acta* **61**, 611–622.

Meckler A. N., Ziegler M., Millán M. I., Breitenbach S. F. M. and Bernasconi S. M. (2014) Long-term performance of the Kiel carbonate device with a new correction scheme for clumped isotope measurements. *Rapid Commun. Mass Spectrom.* **28**, 1705–1715.

Medina B., Guzman H. M. and Mair J. M. (2007) Failed recovery of a collapsed scallop Argopecten ventricosus fishery in Las Perlas Archipelago, Panama. *J. Shellfish Res.* **26**, 9–15.

Meinicke N., Ho S. L., Hannisdal B., Nürnberg D., Tripati A., Schiebel R. and Meckler A. N. (2020) A robust calibration of the clumped isotopes to temperature relationship for foraminifers. *Geochim. Cosmochim. Acta* **270**, 160–183.

Modestou S. E., Leutert T. J., Fernandez A., Lear C. H. and Meckler A. N. (2020) Warm middle Miocene Indian Ocean bottom water temperatures : comparison of clumped isotope and Mg / Ca based estimates. *Paleoceanograpy, Paleoclimatology*.

Müller I. A., Violay M. E. S., Storck J.-C., Fernandez A., van Dijk J., Madonna C. and Bernasconi S. M. (2017) Clumped isotope fractionation during phosphoric acid digestion of carbonates at 70 °C. *Chem. Geol.* **449**, 1–14.

O'Dea A., Hoyos N., Rodríguez F., Degracia B. and De Gracia C. (2012) History of upwelling in the tropical eastern pacific and the paleogeography of the Isthmus of Panama. *Palaeogeogr. Palaeoclimatol. Palaeoecol.* **348–349**, 59–66.

O'Dea A., Lessios H. A., Coates A. G., Eytan R. I., Restrepo-Moreno S. A., Cione A. L., Collins L. S., de Queiroz A., Farris D. W., Norris R. D., Stallard R. F., Woodburne M. O., Aguilera O., Aubry M.-P., Berggren W. A., Budd A. F., Cozzuol M. A., Coppard S. E., Duque-Caro H., Finnegan S., Gasparini G. M., Grossman E. L., Johnson K. G., Keigwin L. D., Knowlton N., Leigh E. G., Leonard-Pingel J. S., Marko P. B., Pyenson N. D., Rachello-Dolmen P. G., Soibelzon E., Soibelzon L., Todd J. A., Vermeij G. J. and Jackson J. B. C. (2016) Formation of the Isthmus of Panama. *Sci. Adv.* **2** e1600883.

Peral M., Daëron M., Blamart D., Bassinot F., Dewilde F., Smialkowski N., Isguder G., Bonnin J., Jorissen F., Kissel C., Michel E., Vázquez R. N. and Waelbroeck C. (2018) Updated calibration of the clumped isotope thermometer in planktonic and benthic foraminifera. *Geochim. Cosmochim. Acta* **239**, 1–16.

Petersen S. V., Defliese W. F., Saenger C., Daëron M., Huntington K. W., John C. M., Kelson J. R., Bernasconi S. M., Colman A. S., Kluge T., Olack G. A., Schauer A. J., Bajnai D., Bonifacie M., Breitenbach S. F. M., Fiebig J., Fernandez A. B., Henkes G. A., Hodell D., Katz A., Kele S., Lohmann K. C., Passey B. H., Peral M. Y., Petrizzo D. A., Rosenheim B. E., Tripati A., Venturelli R., Young E. D. and Winkelstern I. Z. (2019) Effects of improved ^{17}O correction on interlaboratory agreement in clumped isotope calibrations, estimates of mineral-specific offsets, and temperature dependence of acid digestion fractionation. *Geochem. Geophys. Geosyst.* **20**, 3495–3519.

Rodríguez-Sanz L., Bernasconi S. M., Marino G., Heslop D., Müller I. A., Fernandez A., Grant K. M. and Rohling E. J. (2017) Penultimate deglacial warming across the Mediterranean Sea revealed by clumped isotopes in foraminifera. Scientific Reports 7, 16572.

Van Plantinga A. A. and Grossman E. L. (2018) Stable and clumped isotope sclerochronologies of mussels from the Brazos River, Texas (USA): Environmental and ecologic proxy. Chemical Geology 502, 55–65.

Sadatzki H., Alberti M., Garbe-Schönberg D., Andersen N., Strey P., Fortunato H., Andersson C. and Schäfer P. (2019) Paired Li/Ca and $\delta^{18}O$ peaks in bivalve shells from the Gulf of Panama mark seasonal coastal upwelling. *Chem. Geol.* **529** 119295.

Sadler J., Carré M., Azzoug M., Schauer A. J., Ledesma J., Cardenas F., Chase B. M., Bentaleb I., Muller S. D., Mandeng M., Rohling E. J. and Sachs J. P. (2012) Reconstructing past upwelling intensity and the seasonal dynamics of primary productivity along the Peruvian coastline from mollusk shell stable isotopes. *Geochem. Geophys., Geosyst.*, 13.

Saenger C., Affek H. P., Felis T., Thiagarajan N., Lough J. M. and Holcomb M. (2012) Carbonate clumped isotope variability in shallow water corals: Temperature dependence and growth-related vital effects. *Geochim. Cosmochim. Acta* **99**, 224–242.

Schauble E. A., Ghosh P. and Eiler J. M. (2006) Preferential formation of ^{13}C–^{18}O bonds in carbonate minerals, estimated using first-principles lattice dynamics. *Geochim. Cosmochim. Acta* **70**, 2510–2529.

Schauer A. J., Kelson J., Saenger C. and Huntington K. W. (2016) Choice of ^{17}O correction affects clumped isotope (Δ_{47}) values of CO_2 measured with mass spectrometry. *Rapid Commun. Mass Spectrom.* **30**, 2607–2616.

Schmid T. W. and Bernasconi S. M. (2010) An automated method for 'clumped-isotope' measurements on small carbonate samples. *Rapid Commun. Mass Spectrom.* **24**, 1955–1963.

Schmidt G. A. (1999) Error analysis of paleosalinity calculations. *Paleoceanography* **14**, 422–429.

Schöne B. R. (2008) The curse of physiology—challenges and opportunities in the interpretation of geochemical data from mollusk shells. *Geo-Mar. Lett.* **28**, 269–285.

Schöne B. R. and Gillikin D. P. (2013) Unraveling environmental histories from skeletal diaries — Advances in sclerochronology. *Palaeogeogr. Palaeoclimatol. Palaeoecol.* **373**, 1–5.

Schöne B. R., Tanabe K., Dettman D. L. and Sato S. (2003) Environmental controls on shell growth rates and $\delta^{18}O$ of the shallow-marine bivalve mollusk Phacosoma japonicum in Japan. *Mar. Biol.* **142**, 473–485.

Spooner P. T., Guo W., Robinson L. F., Thiagarajan N., Hendry K. R., Rosenheim B. E. and Leng M. J. (2016) Clumped isotope composition of cold-water corals: A role for vital effects? *Geochim. Cosmochim. Acta* **179**, 123–141.

Surge D. M. and Schöne B. R. (2013) Bivalve Sclerochronology. In *Encyclopedia of Scientific Dating Methods* (eds. W. J. Rink and J. Thompson). Springer, Netherlands, Dordrecht, pp. 1–14.

Tao K., Robbins J. A., Grossman E. L. and O'Dea A. (2013) Quantifying upwelling and freshening in nearshore tropical American environments using stable isotopes in modern gastropods. *Bull. Mar. Sci.* **89**, 815–835.

Wacker U., Fiebig J., Tödter J., Schöne B. R., Bahr A., Friedrich O., Tütken T., Gischler E. and Joachimski M. M. (2014) Empirical calibration of the clumped isotope paleothermometer using calcites of various origins. *Geochim. Cosmochim. Acta* **141**, 127–144.

Xie S.-P., Xu H., Kessler W. S. and Nonaka M. (2005) Air–sea interaction over the Eastern Pacific warm pool: cap winds, thermocline dome, and atmospheric convection. *J. Clim.* **18**, 5–20.

Associate editor: Cedric Michael John